Front. Energy 2022, 16(5): 734–746
https://doi.org/10.1007/s11708-022-0840-x

REVIEW ARTICLE

Luis A. ALFONSO-HERRERA, Leticia M. TORRES-MARTINEZ, J. Manuel MORA-HERNANDEZ

Novel strategies to tailor the photocatalytic activity of metal–organic frameworks for hydrogen generation: a mini-review

Abstract This review provides a recompilation of the most important and recent strategies employed to increase the efficiency of metal–organic framework (MOF)-based systems toward the photocatalytic hydrogen evolution (PHE) reaction through specific strategies: tailoring the photocatalytic activity of bare MOFs and guest@MOF composites, formation of heterojunctions based on MOFs and various photocatalysts, and inorganic photocatalysts derived from MOFs. According to the data reported in this mini-review, the most effective strategy to improve the PHE of MOFs relies on modifying the linkers with new secondary building units (SBUs). Although several reviews have investigated the photocatalytic activity of MOFs from a general point of view, many of these studies relate this activity to the physicochemical and catalytic properties of MOFs. However, they did not consider the interactions between the components of the photocatalytic material. This study highlights the effects of strength of the supramolecular interactions on the photocatalytic performance of bare and MOF-based materials during PHE. A thorough review and comparison of the results established that metal–nanoparticle@MOF composites have weak van der Waals forces between components, whereas heterostructures only interact with MOFs at the surface of bare materials. Regarding material derivatives from MOFs, we found that pyrolysis destroyed some beneficial properties of MOFs for PHE. Thus, we conclude that adding SBUs to organic linkers is the most efficient strategy to perform the PHE because the SBUs added to the MOFs promote synergy between the two materials through strong coordination bonds.

Keywords metal–organic frameworks (MOFs), photocatalytic hydrogen evolution, MOF heterojunctions, materials derived from MOFs, bandgap, recombination

Received Jun. 3, 2022; accepted Aug. 12, 2022; online Oct. 20, 2022

Luis A. ALFONSO-HERRERA
Universidad Autónoma de Nuevo León, UANL, Facultad de Ingeniería Civil, Departamento de Ecomateriales y Energía, Av. Universidad S/N Ciudad Universitaria, San Nicolás de los Garza, Nuevo León 66455, México

Leticia M. TORRES-MARTINEZ
Universidad Autónoma de Nuevo León, UANL, Facultad de Ingeniería Civil, Departamento de Ecomateriales y Energía, Av. Universidad S/N Ciudad Universitaria, San Nicolás de los Garza, Nuevo León 66455, México; Centro de Investigación en Materiales Avanzados, S.C. (CIMAV), Miguel de Cervantes No. 120. Complejo Ind. Chihuahua, Chihuahua, Chih 31136, México

J. Manuel MORA-HERNANDEZ (✉)
CONACYT-Universidad Autónoma de Nuevo León, UANL, Facultad de Ingeniería Civil, Departamento de Ecomateriales y Energía, Av. Universidad S/N Ciudad Universitaria, San Nicolás de los Garza, Nuevo León 66455, México
E-mails: jmorah@conacyt.mx; jmmora@live.com.mx

1 Introduction

The use of clean fuels is vital to reduce global warming, and photocatalysis is a promising technology to solve important environmental issues such as global warming, water pollution, and the generation of alternative fuels. Hydrogen is a promising alternative to satisfy increasing global energy requirements because it has high energy efficiency and does not generate hazardous by-products [1]. Hydrocarbon reforming and pyrolysis, which employ fossil fuels as feedstock, are the most commonly employed methods for hydrogen production [2]. Alternative and ecological methodologies for producing hydrogen include electrocatalysis [3] and photocatalysis [4].

Photocatalysis is a powerful tool with high potential to solve some of the most important environmental problems facing humanity; however, there are high barriers to developing efficient photocatalytic systems, such as low photocatalytic efficiency related to the recombination of the charge carrier and poor light absorption under visible light [5,6]. The most commonly employed photocatalysts include inorganic oxides such as

TiO_2 [7], ZnO [8], and $SrZrO_3$ [9]; nevertheless, novel materials such as coordination complexes [10], covalent organic frameworks (COFs) [11], and metal–organic frameworks (MOFs) [12] have been studied for photocatalytic applications.

MOFs are considered hybrid materials because they combine inorganic components (metal ions/clusters) with organic components (linkers). The organic and inorganic elements self-assemble through coordination bonds, producing highly ordered 3d structures (Fig. 1) [13]. There is a wide diversity of MOF materials because thousands of linkers are suitable for constructing MOFs; the most common are carboxylic acids and pyridines [14]. The most outstanding MOF properties are high porosity and large surface area [15]. The synthesis of MOFs with Zn, Cu, Co, Ni, Ti, Zr, Al, and Fe has been reported [16]. MOFs have been employed successfully for photocatalytic hydrogen evolution (PHE) [17], CO_2 reduction [18], and removal of pollutants from water [19]. The PHE mechanism of MOFs begins with light irradiation over the material, which promotes charge carrier separation and electron transfer from the valence band to the conduction band. Depending on the nature of the MOF, linkers, SBUs, or a combination of both, are present in the valence band or the conduction band [20]; thus, light irradiation promotes electron transfer from linkers to metals, from π-π* in linkers, from low-spin to high-spin in metals, or from metals to linkers [21]. The electron transfer produces a hole in the valence band, which oxidizes two water molecules, producing two molecules of oxygen and four protons, and the electrons in the conduction band reduce the protons, producing two hydrogen molecules [22].

Similar to traditional photocatalysts, several MOFs exhibit high charge carrier recombination, poor light absorption in the visible spectrum, and low stability. The poor stability of MOFs compared with that of inorganic materials is one of the main challenges associated with the use of such materials for PHE. The instability is related to the insertion of water into cavities, which replaces linkers and collapses the crystalline lattice [23]. Consequently, creating a hydrophobic environment in the cavities of the MOF is an effective strategy for improving their stability under PHE conditions [24]. This review provides a complete recompilation and analysis of recent studies (2019–2021) that report different strategies for enhancing the photocatalytic activity of MOFs for PHE.

2 Photocatalytic hydrogen evolution

Table 1 describes the recompilation of the different materials in the text, and their hydrogen evolution rates and primary characteristics.

2.1 Tailoring the photocatalytic activity of bare MOFs and guest@MOFs

Bare MOFs have been employed successfully for PHE; however, as mentioned above, the recombination of charge carriers and poor light absorption decreases the efficiency of the MOF. Materials with high crystallinity have higher efficiency for photocatalytic reactions owing to the existence of fewer structural defects [48]. Thus, developing synthesis methods to improve the crystallinity of MOFs is an effective strategy for improving PHE. For example, M-008 (MOF constructed from 4,4-bipyridine and a Zn metal center) has been synthesized using slow evaporation and mechanochemistry. The material synthesized by slow evaporation demonstrated the highest crystallinity, the lowest charge recombination observed in photoluminescence experiments, and the highest hydrogen evolution under UV and visible irradiation [25].

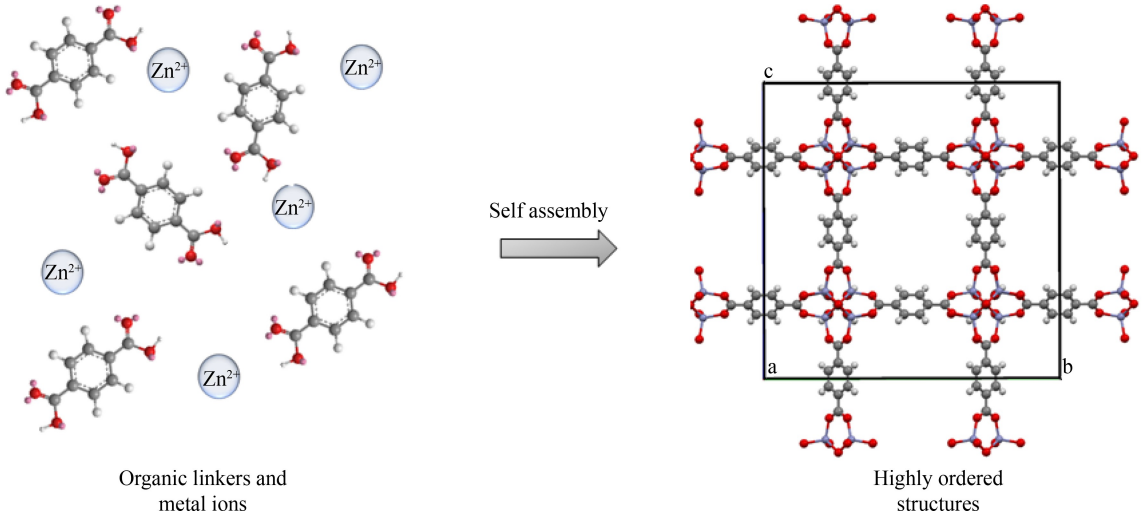

Fig. 1 Self-assembly of schematic linkers and metal ions to form MOFs.

Table 1 Summary of the characteristics, conditions, and photocatalytic hydrogen evolution (PHE) rate for metal–organic framework (MOF) materials described in this review

Strategy to enhance PHE	Strategy	Material	Hydrogen evolution rate/(μmol·(g·h)$^{-1}$)	Light source	Ref.
Tailoring the photocatalytic activity of bare MOFs	Crystallinity effect	M-008A	53	UV light 254 nm	[25]
		M-008B	103		
	Sensitization with Ce^{4+} ions	UiO-67-Ce	269.6	Xe lamp (λ > 400 nm)	[26]
	Pt single-atom encapsulation	MBT	50	300 W Xe lamp (λ > 420 nm)	[27]
		Pt-SACs/MBT	68330		
		Pt-NCs/MBT	44230		
		Pt-NPs/MOF	16410		
	Sensitization with Pt^{4+} ions	PCN-9(Co)	4.8	UV–visible light irradiation	[28]
		PCN-9(Co)-Pt	33.5		
	Self-sensitization	Pt@Pd-PCN-222(Hf)	22674	Visible light ($\lambda \geqslant$ 420 nm)	[29]
	Sensitization with dyes	BDC-Zn	47.5	Solar irradiation	[30]
		BDC-Zn (MO)	1137.8		
		BDC-Zn (MB)	1259.4		
	Sensitization with BODIPY linkers	Pt/CCNU-1	4680	Xenon arc lamp (λ > 420 nm)	[31]
	Sensitization with additional SBUs	$FeBrF_4$@Zr_6-Cu	120000	Visible light (λ = 350–700 nm)	[32]
		mPTCu/Co	11000	Xe lamp 350–700 nm	[27]
		Ti_3-BPDC-Ir	925	Visible light (λ > 400 nm)	[33]
		Ti_3-BPDC-Ru	61		
	Effect of hole position in linkers	NH_2-MIL-125-Ti	1.5	UV light (λ = 240–400 nm)	[34]
		MIL-125-Ti	57.7		
Formation of heterojunctions based on MOFs and various photocatalysts	Coupled with g-C_3N_4	g-C_3N_4 /UMOFNs	1909	500 W Xe lamp (λ = 250–1800 nm)	[35]
		NH_2-MIL-125/g-C_3N_4	5316	300 W Xe (λ > 400 nm)	[36]
	Morphology effect of material	CZS/NMF-4	1713.2	5 W LED	[37]
	Exposed crystallographic plane effect	TiO_2@MOF FS	44	Sum of light illumination (300 W Xe lamp)	[38]
	Co-catalyst encapsulated in MOFs pores	ZIF-8/MoS_2	68.4	Solar light simulator	[39]
	Heterostructures associated by covalent bonds	MOF-808@TpPa-1-COF (6/4)	11880	Summed light illumination (300 W Xe lamp)	[40]
Inorganic photocatalyst derived from MOFs	Carbonaceous materials synthesized from MOFs	$Cd(OH)_2$/CdS 40-gCN-NPC	148.13	Solar light (150 W Xe lamp)	[41]
		Ni_2P/Ni@C/g-C_3N_4-550	8040	300 W Xe lamp ($\lambda \geqslant$ 420 nm)	[42]
	Free noble metal heterostructures	NiS(0.3%)/CdS(30%)/TiO_2	2149.15	300 W Xe lamp ($\lambda \geqslant$ 420 nm)	[43]
	Inorganic heterostructures from MOF core-shell structures	CdS/MoS_2	5587	300 W Xe lamp	[44]
		Cu_3P@CoP	9399	UV–visible light irradiation Simulated solar light 5 W LED white-light multi-channel	[45]
	Ru single-atom encapsulation into carbonaceous materials	Ru-NPs/SAs@N-TC	5000	300 W Xe lamp (λ = 320–780 nm)	[46]
	Cu adsorption in the MOF derivative surface	Cu/C-ZnO	5363.3	300 W Xe lamp. UV cut-off filter (λ < 420 nm)	[47]

Photosensitization with organic dyes is an interesting strategy for improving light absorption under the visible spectrum. Several MOFs have a high capacity to adsorb organic dyes; however, few reports have related this property to the sensitization phenomenon. BDC-Zn (a MOF containing terephthalic acid and Zn) was evaluated for PHE under visible spectra and demonstrated poor photocatalytic activity; nevertheless, the photocatalytic activity was considerably improved in the presence of methyl orange (MO). The high sensitization by MO is related to the high capacity of the BDC-Zn MOF to adsorb this dye [30].

The location of the holes in the linkers under light irradiation plays an important role in reducing charge carrier recombination. The holes of MIL-125-Ti (a MOF containing Ti and terephthalic acid synthesized using the

solvothermal method) reside in the O2p band in the linkers, whereas electrons are localized in the metallic center. As the distance between O2p and Ti is very short, recombination issues occur rapidly. However, when MIL-125-Ti is functionalized with an amine group (-NH_2), holes exist in the N atoms. Because the N-Ti bond is longer than O-Ti bond, the recombination issues are reduced. Nevertheless, in the presence of sacrificial agents, MIL-125-Ti exhibits higher photocatalytic activity than H_2N-MIL-125-Ti because of the short distance between the holes and the metallic center in which the sacrificial agent is adsorbed. XRD experiments indicated that both materials undergo important changes in their crystalline phases after 1 h under PHE conditions; in particular, TEOA promotes the degradation of the material, indicating poor stability [34].

There are several examples of linker-type coordination compounds that have high potential to improve light absorption. A series of FeX@Zr_6Cu MOFs synthesized through an evaporation method comprises photosensitizing linkers (Cu-PSs) and highly active Fe^{2+} redox sites supported on secondary building units (SBUs). The visible spectra of FeX@Zr_6Cu indicates high PHE activity, which was attributed to the proximity (~1 nm) of the Cu-PSs to the SBUs. In addition, Fe^{2+} is stabilized by periodically ordered SBUs. The synergy between Cu-PSs and SBUs occurs by Cu-PS excited state quenching by 3-dimethyl-2-phenyl-2,3-dihydro-1Hbenzo[d]-imidazole (BIH, a sacrificial agent) to afford the $[Cu\text{-}PS]^-$ species, which sequentially injects two electrons to the Fe^{2+} site to generate the Fe^{2+}–H intermediate for photocatalytic H_2 evolution [32]. Notably, the FeX@Zr_6Cu MOFs have efficient PHE activity for 80 h, indicating high stability. The visible spectra of two MOFs, mPTCu/Co and mPTCu/Re, synthesized using a solvothermal method, reveal high activity toward the PHE, similar to that reported in the previous study [27]. This activity was attributed to the proximity of the SBUs Cu-PSs to the active Co/Re catalyst. The high activity of these materials is related to their reductive quenching pathway, as determined by photophysical and electrochemical experiments. The photo-excited [Cu-Ps]* species are quenched by BIH (sacrificial agent), producing $[Cu\text{-}Ps]^-$ species, which transfer electrons to the Co/Re photocatalytic sites where the PHE is carried out. The photocatalytic cycle is illustrated in Fig. 2. Notably, the mPTCu/Co and mPTCu/Re MOFs had efficient PHE activity for 72 h, indicating high stability [49].

In another example of the sensitization of MOFs with additional SBUs, the titanium-based material Ti_3-BPDC, synthesized through a solvothermal reaction, was doped with $[Ir(ppy)_2(dcbpy)]Cl$ or $[Ru(bpy)_2(dcbpy)]Cl_2$ (bpy = 2,2′-bipyridine, ppy = 2-phenylpyridine, dcbpy = 2,2′-bipyridine-5,5′-dicarboxylate) to obtain Ti_3-BPDC-Ir and Ti_3-BPDC-Ru. The PHE was improved because the hierarchical assembly of photosensitizer linkers and Ti clusters facilitates the charge carrier transfer, enhancing light absorption and reducing charge carrier recombination. In the photocatalytic cycle, $[Ir(ppy)_2(dcbpy)]^+$ is photo-excited to $[Ir(ppy)_2(dcbpy)]^{+*}$, which is subsequently reduced by BIH to $[Ir(ppy)_2(dcbpy)]$; these species transfer electrons to the Ti cluster, where the PHE is carried out, and simultaneously, $[Ir(ppy)_2(dcbpy)]^+$ is regenerated (Fig. 3). The authors analyzed the RXD patterns of Ti_3-BPDC-Ir and Ti_3-BPDC-Ru after PHE (72 h); and found that no changes occurred in the crystalline phase of the materials, indicating high stability [33].

The infiltration of guest molecules into MOFs is an effective strategy to modulate important physicochemical properties, such as the bandgap, that improve PHE [50].

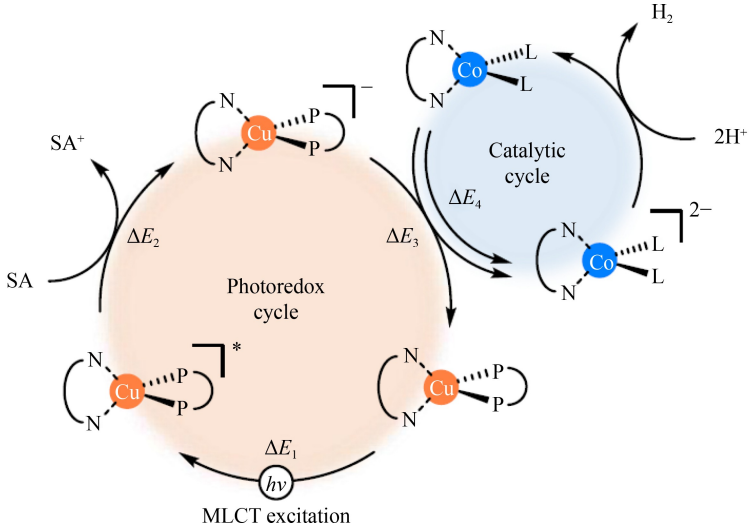

Fig. 2 Proposed catalytic cycle for mPTCu/Co-catalyzed for the PHE (adapted with permission from Ref. [49]).

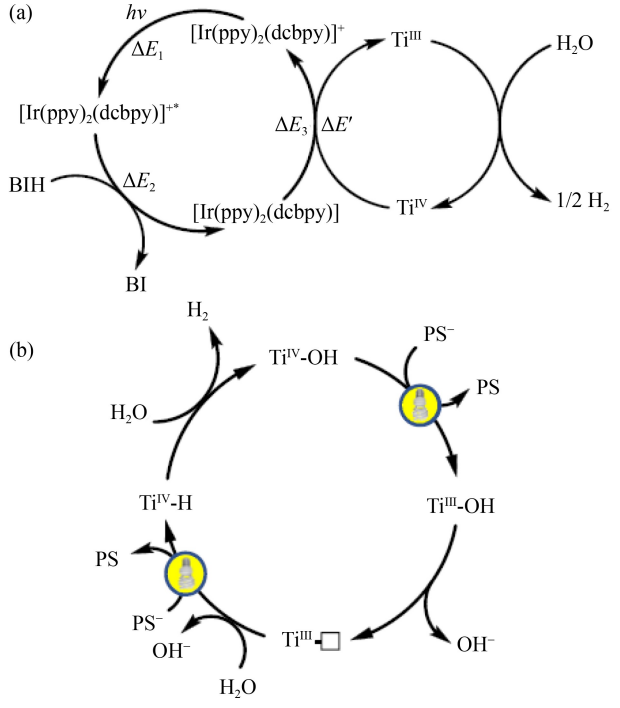

Fig. 3 (a) Proposed catalytic cycle for the visible light-driven PHE catalyzed by Ti_3-BPDC-Ir; (b) detailed catalytic mechanism of the reaction on the Ti site via the Ti^{IV}/Ti^{III} cycle (adapted with permission from Ref. [33]).

In addition, guest molecules can promote charge transfer between the host and guest, thereby reducing recombination [51]. Guest molecules can be encapsulated during the synthesis process or through a post-synthesis methodology. Encapsulation through synthesis is performed via a one-pot synthesis method in which guest molecules are encapsulated, while linkers and metals are self-assembled. The one-pot synthesis method has advantages over post-synthesis methodologies [52]; for example, the guest molecules are more homogeneously distributed inside the MOF and the guest molecules penetrate deeper into the MOFs [52]. In addition, materials that are infiltrated through the one-pot synthesis methodology usually retain their crystallinity and crystal phase [53,54]. Infiltration through post-synthesis methodologies requires pretreatment, during which the residual solvent is removed from the MOFs. In post-synthesis methodologies, the encapsulation of guest molecules can be carried out from a liquid solution or gas/vapor phase. Usually, encapsulation from a gas/vapor phase is advantageous over encapsulation from a liquid phase because there is no competition between the solvent and guest molecules in the former [55]. Cerium is a lanthanide that usually exhibits activity under visible light irradiation owing to its electronic configuration. Therefore, cerium is useful for improving the light-harvesting ability of MOFs. Other lanthanides and actinides can also enhance the optical properties of MOFs. Platinum is a highly conductive element that is useful for improving the mobility of electrons toward the surface of the material. Another reported strategy to improve light absorption and reduce charge carrier recombination relies on infiltrating the MOF with metal cations such as Ce^{4+}, an effective photosensitizer, or Pt^{4+}, a highly conductive metal. Ce^{4+} cations were introduced to the crystal structure of UIO-67 (a Zr-based MOF with biphenyl-4,4-dicarboxylic (bpdc) acid as a linker), partially replacing the bpdc linkers with 2,2-bipyridine-5,5-dicarboxylic acid (bpydc). The nitrogen groups in the bpydc linkers have a high capacity to form coordination bonds with Ce^{4+} cations; thus, Ce^{4+} is easily incorporated into UIO-67 following this methodology. The authors synthesized the UIO-67 material using a solvothermal reaction, whereas encapsulation of Ce^{4+} was carried out using a one-pot method. The photocatalytic activity of the modified material is 10 times higher than that of bare UIO-67, which reduces the recombination rate caused by charge transfer from the bpdc linkers to the bpydc-Ce^{4+} linkers. After 6 h of light irradiation, the authors observed a decrease in the PHE rate for the bare material and composite, indicating low stability [26]. PCN-9 (a MOF containing Co and 2,4,6-tris(4-carboxyphenyl)-1,3,5-triazine) was modified by the adsorption of Pt^{4+} ions. The cations were incorporated into PCN-9 through coordination bonds with nitrogen atoms in the triazine linkers. The authors synthesized PCN-9 using a solvothermal reaction and encapsulated Pt^{4+} ions using a simple method of adsorption from a solution with different concentrations of Pt^{4+}. The resulting materials demonstrated less charge carrier recombination than bare PCN-9 because the photogenerated electrons in the organic linkers were transferred to Pt, avoiding recombination. High stability was observed in the modified material in X-ray photonelectron spectroscopy (XPS) experiments [28]. XPS experiments indicated that the Pt^{4+} encapsulated in PCN-9 had the same oxidation state after the photocatalytic experiments, suggesting high stability.

Single-atom encapsulation into MOF pores is another interesting approach for decreasing charge carrier recombination in MOFs. For example, the single-ion trap method involves the encapsulation of Pt atoms in MOF-808 (a MOF containing Zr and trimesic acid synthesized by the solvothermal reaction). The original formate linkers bonded to Zr clusters were exchanged with EDTA linkers, Pt^{2+} ions were coordinated to EDTA linkers, and the resulting material was heat-treated at 200°C under H_2 atmosphere to produce single Pt atoms. The modified MOF demonstrated a lower charge carrier recombination than bare MOF-808, which improved the PHE reaction. MOF-808 modification has an outstanding quantum efficiency of 67.6% at 420 nm [27]. The PHE activity of Pt@MOF-808 did not decrease after five reaction cycles (25 h), indicating exceptional stability.

MOFs synthesized from porphyrin linkers can

demonstrate self-sensitization; this occurs in Pd-PCN-222(Hf), a MOF constructed from the palladium (II) meso-tetra (4-carboxyphenyl) porphyrin linker. Such porphyrin linkers coordinated to Hf clusters produce large pores (3.7 nm), where Pt nanoparticles are inserted to play the role of the co-catalyst. The authors synthesized a pristine PCN-222(Hf) MOF using a solvothermal reaction and encapsulated Pt nanoparticles using an adsorption methodology promoted by sonication. In addition to excellent light absorption in the visible spectrum, Pt@Pd-PCN-22(Hf) showed an unprecedented PHE rate of 22674 μmol/(g·h), which is attributable to a synergistic effect between the Pd-porphyrin linkers and Pt nanoparticles. The bare material and composite were immersed in different solvents (methanol, acetonitrile, acetone, dichloromethane, ethyl acetate, and water). After seven days, neither Pd-PCN-222(Hf) nor Pt@Pd-PCN-22(Hf) exhibited changes in their crystallinity and crystal phase, indicating exceptional stability. In addition, the materials were stable in an aqueous solution at a pH of 1–12 for 24 h. The authors attributed the outstanding stability of Pd-PCN-222(Hf) and Pt@Pd-PCN-22(Hf) to the hydrophobic environment resulting from the presence of Hf clusters [29].

Another strategy to improve the light absorption in MOFs is photosensitization using organic compounds and the addition of SBUs to linkers. For example, Yang et al. [31] synthesized the MOF CCNU-1 (constructed from a Zn metal center and two linkers, BDPC, and BODIPY) using a solvothermal method. In addition, the authors encapsulated Pt nanoparticles using an adsorption methodology with an aqueous solution and $NaBH_4$ as a reducing agent. The excellent light adsorption properties of BODIPY (4,4-difluoro-4-bora-3a,4a-diaza-s-indacene) have been widely reported; therefore, the addition of this linker to MOFs results in an interesting method to increase light absorption. BODIPY-based CCNU-1 is the first MOF reported in the literature to present a high efficiency for light absorption in the 200 to 800 nm range. The Pt@CCNU-1 composite has an efficient PHE rate of 420 nm with an apparent quantum efficiency of 9.06%. The authors immersed the CCNU-1 MOF in aqueous solutions with a pH between 1 and 11; subsequently, XRD experiments indicated that CCNU-1 did not change its crystalline phase and crystallinity. In addition, after three PHE cycles (9 h), the materials did not exhibit a decrease in the PHE rate, indicating high photostability. The authors attributed the high CCNU-1 stability to the strong coordination bond of N–Zn [31].

In addition to inorganic nanoparticles, metallic sulfides can be encapsulated by the pores of MOFs to produce an efficient photocatalyst for PHE. For example, MoS_2 was encapsulated in a zeolitic imidazolate framework-8 (ZIF-8) via a one-pot synthesis method and the resultant heterostructure was evaluated for PHE. ZIF-8 has a suitable band edge position for the PHE; however, this MOF exhibits poor light absorption in the visible spectrum. In contrast, MoS_2 exhibits excellent light absorption under visible light but an unsuitable band structure position for the PHE. After exfoliation, MoS_2 was encapsulated in the pores of ZIF-8. The heterostructure of ZIF-8@MoS_2 exhibits enhanced light absorption under visible spectra compared to bare ZIF-8. Additionally, the band structure position of ZIF-8 was not modified; such characteristics improve the PHE under visible light [39].

In this section, we present strategies for enhancing the PHE in MOFs by tailoring their properties, such as crystallinity and adsorption capacity. We also present strategies for tailoring the structural properties of MOFs, such as the use of highly conjugated linkers, the extension of linkers through the addition of organometallic/coordination compounds, and control of the charge carrier position through the addition of functional groups. In addition, we summarize previous studies that involve the encapsulation of different species inside MOFs to increase their PHE activity. A remarkable strategy, efficient charge separation is crucial for developing materials for efficient PHE. The extension of linkers by adding new SBUs or encapsulating metallic species is an efficient strategy to enhance the PHE because it promotes charge transport between the two components of the same material. This phenomenon is not observed in MOFs with enhanced macroscopic or structural properties, such as crystallinity or highly conjugated linkers, because charge transport occurs within the same component. Regarding sensitization with additional SBUs, the short distance between SBUs was responsible for the outstanding results. We believe that the coordination bond between the functional groups in the linkers and additional SBUs is a key factor for producing high PHE activity because it is an interaction stronger than VWFs, which are usually present in metallic-nanoparticle@MOF composites. Regarding the stability parameter, most of the analyzed compounds are highly stable under PHE conditions. We believe that the encapsulation of metallic nanoparticles prevents water infiltrating the pores of the MOF, which usually alters the crystalline lattice. Furthermore, additional SBUs promote the formation of a hydrophobic environment inside the cavities of the MOF, resulting in high stability.

2.2 Formation of heterojunctions based on MOFs and various photocatalysts

Heterostructures are material configurations capable of improving the charge carrier transfer of bare materials according to the band position of each bare material, thus reducing recombination issues and increasing PHE activity. The driving force for these specific configurations is the transfer of charge carriers from high

to low energy levels under light irradiation. Thus, the holes in the valence band migrate from a higher energy level to the valence band with the lowest oxidation potential on the other semiconductor, whereas electrons migrate from the conduction band with a high energy level to the conduction band with the lowest reduction potential (heterostructure types I and II) or to the valence band of the coupled semiconductor (heterostructure types III and Z-scheme) [56]. Heterostructures can also be classified according to the arrangement and interface of different semiconductors, for example, a) spherical zero-dimensional, b) cylindrical one-dimensional, c) planar two-dimensional, and d) cubic three-dimensional [57].

Graphitic carbon nitride (g-C_3N_4) is a promising photocatalyst for PHE because it has excellent optical properties and is inexpensive and environmentally friendly. Nevertheless, several challenges limit the use of g-C_3N_4 on an extensive scale. For example, g-C_3N_4 is usually synthesized through the molten salt method, which produces a 2d morphology associated with small surface area [58]. Other synthesis methods produce g-C_3N_4 with interesting morphologies associated with a large surface area; nevertheless, a large surface area can produce vacancies and structural defects that can reduce the efficiency of g-C_3N_4 for PHE [59]. Consequently, coupling g-C_3N_4 with a non-precious co-catalyst is essential to overcome the aforementioned problems to develop an efficient PHE system based on g-C_3N_4 [60]. Thus, we believe that MOFs have high potential for synergy with g-C_3N_4. The limiting 2d structure of g-C_3N_4 can promote π-stacking interactions with MOFs, which results in large surface areas and crystallinity. Several MOFs, such as ZIF-8, produce large bandgaps (~5 eV) [61]; thus, g-C_3N_4 can be used to improve the light harvesting of MOFs. For example, 2d Co-Ni-based MOFs (UMOFNs) were coupled to g-C_3N_4 by a simple mechanochemical grinding method. The resultant heterostructure has better light absorption and results in lower charge carrier recombination than bare materials. The enhanced PHE efficiency is attributable to the 2d–2d UMOFNs and g-C_3N_4 morphology, which reduces the distance between materials and improves the charge transference processes. The highly dispersed Ni-O, Co-O, and π-π bonds in UMOFNs with 2d–2d structures promoted and improved the charge transfer and photocatalytic activity. The authors indicated that after 10 reaction cycles, the PHE of UMOFNs/g-C_3N_4 decreased by 20%; they attributed the loss of PHE to a slight loss in the catalyst recovery process or the separation of the heterostructure components. After the reaction cycle, the authors observed that the XRD results for g-C_3N_4 did not reveal any important changes, indicating that the catalyst has high stability. Nevertheless, the peaks representing UMOFNs are not observed. Therefore, analyzing the global stability of the heterostructure is difficult. In another study, Ti-MOFs (TiATA) were coupled to g-C_3N_4 using a mechanochemical process and subsequent annealing. XPS analysis revealed the presence of the C-Ti bond, suggesting that the C in g-C_3N_4 interact with Ti metal centers in TiATA. The interactions between both materials improves the light absorption of g-C_3N_4 and reduces the charge carrier recombination. Photocatalysis suggests that electrons migrate from g-C_3N_4 to TiATA and then to Pt nanoparticles (co-catalyst) supported on the heterostructure surface to carry out the PHE [36].

In addition to the properties of the compound, the morphology of the material plays a crucial role in constructing heterostructures with high efficiency for the PHE. For example, 0D $Cd_xZn_{1-x}S$ was coupled to a 2d Ni-MOF-74 via a simple hydrothermal and physical mixing method to construct the heterostructure CZS/NMF-4; the 0 and 2d space structure reduced the agglomeration of CSZ on the NMF-4 surface, which increased the available active photocatalytic sites for hydrogen evolution. The synergy between CSZ and NMF-4 produces photocatalytic activity 10 times higher than that of bare materials. After four reaction cycles (20 h), the PHE rate of CZS/NMF-4 decreased from 1713.2 to 1102.2 μmol, indicating low stability. XRD experiments indicated that the crystal phase of CZS did not show significant changes after the photocatalytic reaction, whereas the before and after XRD patterns of NMF-4 contrasted markedly, indicating that NMF-4 was responsible for the low heterostructure stability [37].

Polycrystalline materials interact through different crystallographic planes, and some crystallographic planes are more active than others toward PHE. Thus, conserving the most active crystallographic planes available to interact with the reaction medium in a core-shell heterostructure is desirable. MIL-125 (Ti) has four different facets: {110}, {100}, {001}, and {111}, with {100} being the most active. This plane has a high affinity for electron-rich species such as tannic acid, so this molecule can be used to protect the {100} plane and construct the core-shell structure TiO_2@NH_2-MIL-125(Ti). The resultant heterostructure has a tight heterojunction interface between TiO_2 and NH_2-MIL-125(Ti) while maintaining the open diffusion channels of NH_2-MIL-125(Ti), which improves the electrical conductivity and light absorption, and therefore, the PHE under visible light irradiation (Fig. 4). The TiO_2@NH_2-MIL-125 (Ti) composite maintained its PHE rate over five reaction cycles (50 h), indicating high stability [38].

A novel approach for constructing heterostructures involves assembling two materials through covalent bonds. COFs are coupled to MOFs via a Schiff base reaction using free amine groups in the MOF linkers. In addition, post-synthetic modifications in clusters can be used to construct core-shell MOF@COF structures. For example, MOF-808 (a material composed of Zr and 1,3,5-benzene tricarboxylic acid) has been modified by coordinating p-aminobenzoic acid in Zr clusters. The

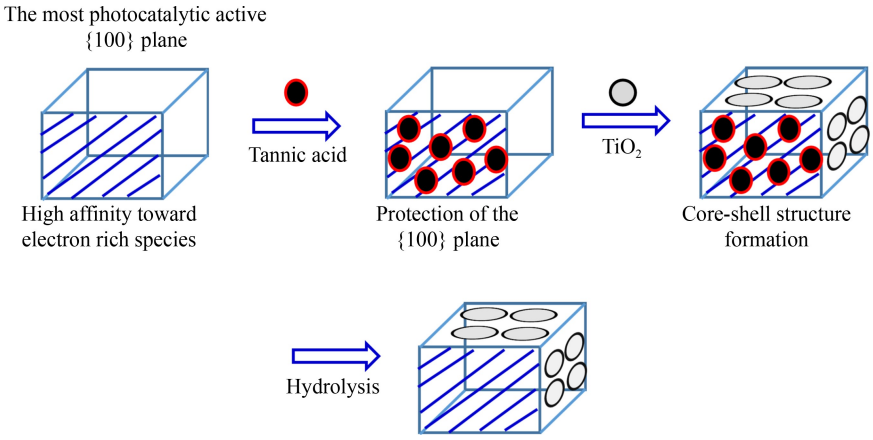

Fig. 4 Schematic protection of the most active {100} crystallographic plane and core-shell structure formation.

modified material had sites available to form covalent bonds with TpPa-1-COF. The resultant heterostructure exhibited photocatalytic activity 5.6 times higher than that of bare TpPa-1-COF, which was attributed to the efficient charge carrier separation and transport associated with the MOF–COF covalent bond [40].

In this section, we present strategies based on the formation of heterostructures to increase the PHE of MOFs. We present an MOF with organic compounds, such as COFs and g-C_3N_4, and inorganic components, such as TiO_2. As mentioned previously, understanding the interactions between the components of the heterostructure is crucial for understanding and comparing the different hydrogen evolution efficiencies observed in each study. Thus, the inorganic-component/MOF heterostructures exhibited the lowest efficiency. This was attributed to the weaker supramolecular (most likely van der Waals) forces at the surface of the component. In addition, the heterostructure g-C_3N_4/MOF is more efficient than materials fabricated with inorganic materials; we attribute this to the 2d morphology of MOFs and g-C_3N_4, which produces supramolecular interactions stronger than van der Waals forces. This means that MOFs with other morphologies probably do not couple as efficiently as 2d MOFs with g-C_3N_4. The heterostructure MOF@MOF/TiO_2 has an enhanced PHE efficiency; nevertheless, it is worth mentioning that this is a ternary structure in which the core-shell MOF component interacts through strong coordination bonds. MOF-808@TpPa-1-COF (6/4) had the most efficient PHE rate, which was consistent with its strongest supramolecular interaction (covalent bond). Notably, the heterostructures discussed in this section had lower PHE rates than the guest@MOF composites. We attribute this behavior to the supramolecular interactions of guest molecules with the MOFs occurring in each MOF cavity. In contrast, the interactions between the components of heterostructures occur only on the surface, resulting in less efficient charge transport. The heterostructures had lower stability than the guest@MOFs and MOFs with additional SBUs. We believe that the accessible cavities in the MOFs allow water to infiltrate, which replaces the organic linkers in the SBUs, leading to the collapse of the framework. The exception to the previous statement was TiO_2@NH_2-MIL-125(Ti), which had a core-shell structure in which TiO_2 surrounded the MOF material, probably decreasing the contact between water and the MOF material.

2.3 Inorganic photocatalyst derived from MOFs

A useful strategy for developing inorganic materials for highly efficient PHE involves utilizing MOFs as templates. The pyrolysis of MOFs produces an inorganic oxide corresponding to the metal center. In addition, carbonaceous materials can be obtained from MOFs using this methodology. For example, g-C_3N_4 is an interesting material for PHE; however, similar to other photocatalysts, it suffers from charge carrier recombination issues, which decrease its photocatalytic efficiency. The photocatalytic efficiency was improved by synthesizing a ternary heterostructure composed of g-C_3N_4, Cd-based compounds (Cd_x: $Cd(OH)_2$, CdS, and CdO), and mesoporous carbon flakes (MCFs). The synthesis of MCFs consists of three steps: synthesis of Al-MOF, carbonization of Al-MOF, and removal of Al with HCl solution. Moreover, the authors coupled the components of the ternary heterostructure using a wet impregnation method. Carbon flakes synthesized from Al-MOFs have small particle sizes (12–22 nm) and large surface areas (809 m^2/g). Because MCFs can act as electron acceptors, the resultant heterostructure has a narrow bandgap, which improves the light absorption and lowers the overpotential to carry out the hydrogen evolution reaction, as well as low charge carrier recombination. Notably, the heterostructure did not exhibit a decrease in the PHE rate after five reaction cycles (20 h), indicating high stability [41].

Similarly, Ni_2P/Ni nanoparticles encapsulated in carbon/g-C_3N_4 were synthesized *in situ* by the pyrolysis and phosphatization of Ni-MOF. The Ni_2P/Ni@C/g-C_3N_4-550 heterostructure was evaluated for PHE using Eosin-Y (EY) as a sensitizer. The material exhibited an apparent quantum efficiency of 58.1% at 420 nm. This positive result was attributed to carbon, which acts as an electron transport bridge between EY and Ni_2P/g-C_3N_4, thus accelerating the proton reduction reaction on the Ni_2P/Ni NPs. A schematic of the process used to construct this composite is shown in Fig. 5. After five PHE cycles (25 h), the authors observed a slight decrease in the PHE rate, indicating good stability [42].

Free noble metal heterostructures with high efficiency for the PHE have been constructed using MOFs as templates. NiS/CdS/TiO_2 (NS/CT) was synthesized from the NH_2-MIL 185 MOF. In the first step, NH_2-MIL 185 MOF was impregnated with Cd^{2+} ions using an adsorption process. CdS/h-TiO_2 was synthesized using a one-step sulfurization method employing thioacetamide as the sulfur source. Finally, modified NiS/CdS/TiO_2 (NS/CT) was synthesized using the photodeposition method. The high PHE efficiency was attributed to the fast charge separation promoted by the NiS co-catalyst. After four PHE cycles (16 h), the authors observed a slight decrease in the PHE rate, indicating good stability [43].

Inorganic heterostructures have been constructed from core-shell materials that coat MOFs with inorganic materials. For example, MoS_2 flowers were coated with a Cd-based MOF to construct a core-shell material. The coated MOF was sulfurized with thioacetamide to form an inorganic heterostructure CdS/MoS_2 with high efficiency for PHE; the improvement was attributed to the large surface area and intimate contact between CdS and MoS_2, which enhanced the charge transfer and decreased the charge carrier recombination. The large CdS/MoS_2 surface area is produced by the highly ordered Cd^{2+} structure separated by organic linkers. The authors concluded that the heterostructure CdS/MoS_2 had poor stability as a result of the photocorrosion of CdS during the photocatalytic reaction [44].

Core-shell structures can also be synthesized by combining the two MOFs. Cu-MOFs@ZIF-9(Co) synthesized at room temperature by a stirring method were used to construct the heterostructure Cu_3P@CoP by employing low-temperature phosphorization. The heterostructure Cu_3P@CoP has a large surface area, hierarchical structure, and a p-n heterojunction at the interface. Photoelectrochemical and fluorescence experiments showed that the charge transfer between Cu_3P and CoP is thermodynamically favorable, reducing the recombination of charge carriers and thus enhancing the PHE. After four PHE cycles (20 h), the authors observed a slight decrease in the PHE rate, indicating good stability [45].

An effective strategy to support noble metals in carbonaceous materials is to adsorb metals onto MOFs and then use pyrolysis to transform the initial material into a carbonaceous derivative. For example, Ru single atoms were embedded in NH_2-MIL-125 and then subjected to pyrolysis to synthesize Ru-NPs/SAs@N-TC and Ru-SAs@N-TC. The morphology and structure of N-TC (a derivative of NH_2-MIL-125) depend on the initial quantity of Ru^{3+} and the final size and dispersion states of Ru. Ru-NPs/SAs@N-TC had higher photocatalytic activity than Ru-SAs@N-TC, which was attributed to a large surface area and synergistic coupling effect between the Ru nanoparticles and Ru single atoms. After three PHE cycles (9 h), the authors observed no decrease in the PHE rate, indicating a high stability. In addition, LSV experiments performed before and after 1000 CV cycles

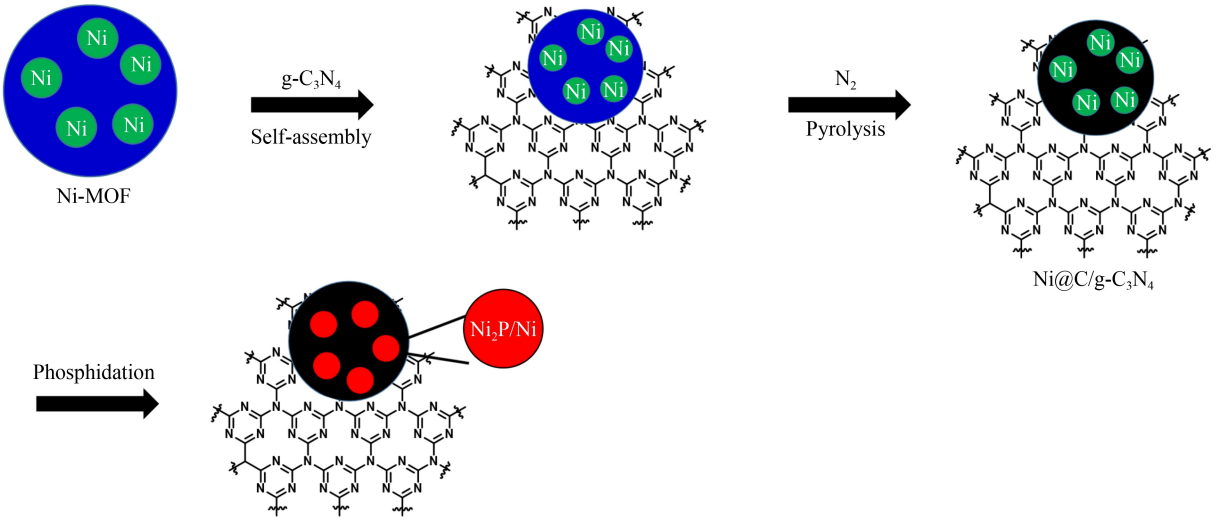

Fig. 5 Formation of Ni_2P/Ni@C/g-C_3N_4 composites.

revealed a similar electrochemical response, confirming the high stability of Ru-SAs@N-TC [46].

The photocatalytic activity of MOF inorganic derivatives can be enhanced by the adsorption of cationic metals on the surface of the material. Following the photoreduction method, copper was loaded onto C-ZnO synthesized from MOF-5 obtained from a solvothermal reaction (MOF containing Zn and terephthalic acid). The Cu/C-ZnO material has a narrow bandgap associated with oxygen vacancies and a high electron density at the Fermi level produced by C atoms. In addition, the structure of the material improved the charge carrier separation and transport. Cu incorporation on the surface of the material increased the photocatalytic activity of C-ZnO by 9663 times. After five PHE cycles (16 h), the authors observed a slight decrease in the PHE rate, indicating good stability [47].

In summary, inorganic materials derived from MOFs usually exhibit high efficiency toward PHE. The pyrolysis of MOFs usually produces inorganic materials doped with carbon or carbonaceous materials doped with metals. The interactions between the metals or carbon with the material derivative from the pyrolysis of MOFs should occur through strong interactions, such as covalent or ionic bonds, because the metals are doped into the crystalline lattice, which results in an efficient charge transfer that can modulate the bandgap value or reduce recombination. Notably, we analyzed materials derived from MOFs that are used to construct secondary and ternary heterostructures. Therefore, pyrolysis was combined with the strategy presented in the previous section, explaining the high efficiency toward PHE of MOF derivatives compared with heterostructures based on MOFs. Notably, the materials derived from MOFs had a lower efficiency than several composite guest@MOFs, indicating that pyrolysis affects some properties of MOFs that are crucial for PHE, such as large surface area and stability. Generally, the stability of MOF derivatives is higher than that of pristine materials because inorganic compounds usually have stronger bonds than organic compounds. Nevertheless, some material derivatives from MOFs, such as metallic sulfides, exhibit poor stability, even when compared with the pristine MOFs presented in Section 2.1.

3 Conclusions

The coupling of MOFs with other non-photocatalysts, such as metal ions, metal nanoparticles, or single metal atoms, results in excellent PHE. The sensitization of MOFs by dye adsorption and the increase in the degree of crystallinity are effective strategies for enhancing the PHE in bare MOFs. The photocatalytic improvement of the heterostructure MOF-photocatalyst is caused by the remarkable synergy between the MOFs and g-CN. However, it is important to note that the morphology also plays a decisive role in producing effective coupling. In general, inorganic semiconductor derivatives of MOFs exhibit efficient PHE because these materials usually have high durability. Composite-type guest@MOFs are highly efficient for the PHE because the encapsulation of guest molecules promotes charge transfer between the composite components, thereby reducing recombination. Linkers with additional SBUs have excellent light absorption in the visible spectrum, and closer proximity between active sites improves the charge carrier transfer, decreasing the recombination rate. We compared the strategies presented in this mini-review, and we conclude that the interactions between MOFs and other species are crucial for understanding and enhancing the efficiency of MOF-based photocatalysts toward PHE. Guest@MOF composites have a higher PHE efficiency than heterostructure-based MOFs because the interactions between guest molecules and MOFs occur in the cavities of the guest@MOF. In contrast, in heterostructure-based MOFs, interactions only occur on the surface of the material.

The pyrolysis of MOFs is an interesting procedure for obtaining inorganic materials (oxides and carbonaceous materials) derived from MOFs, which have a higher PHE efficiency than heterostructured MOFs because these inorganic materials are homogeneously doped with carbon or metals through strong ionic or covalent bonds and are usually employed to construct heterostructures. The pyrolysis of MOFs involves two strategies: the development of C/metal@inorganic materials and the construction of heterostructures. Inorganic materials derived from MOFs have lower PHE rates than several guest@MOFs and MOFs with additional SBUs, indicating that pyrolysis damages some important properties of MOFs associated with PHE, such as the large surface area or high stability. The addition of SBUs is the best strategy for obtaining an efficient photocatalyst because it increases the number of active sites of the MOFs through strong coordination bonds, promoting efficient light capture and charge transport.

Guest@MOFs demonstrated the highest stability due to prevention of water infiltration. Other MOF types discussed in this review allowed water to infiltrate their cavities, replacing linkers and promoting the collapse of the crystal lattice. We believe that future investigations of MOFs for PHE should focus on understanding and controlling the interaction between MOFs and other materials.

Although the modulation and enhancement of the structural and macroscopic properties of MOFs can be useful to increase light harvesting for PHE applications, we believe it is essential to relate the strength of the interactions between the components forming a MOF heterostructure or a MOF composite with the

recombination rate, as the enhancement of the charge carrier transfer rate is related to a strong interaction that reduces the distance between the material components. Thus, single-crystal XRD or computational experiments are tools that allow the specific interactions in guest@MOF to be studied in relation to their photocatalytic properties. However, while studying the interactions that govern heterostructures on MOFs remains a challenge, the research performed in this field to date shows significant promise.

Acknowledgments This work was supported by CONACYT through the following projects: Cátedras CONACYT—ID7708, CONACYT-FC-1725. Luis. A. Alfonso-Herrera thanks CONACYT for the M.C. scholarship 844207. UANL also supported this research through projects PAICYT CE1352-20 and PAICYT 601-CE-2022.

Notations

MOF	Metal–organic framework
PHE	Photocatalytic hydrogen evolution
COF	Covalent organic framework
bpdc	Biphenyl-4,4-dicarboxylic acid
bpydc	2,2-bipyridine-5,5-dicarboxylic acid
XPS	X-ray photoelectron spectroscopy
EDTA	Ethylenediaminetetraacetic acid
SBU	Secondary building unit
BIH	3-dimethyl-2-phenyl-2,3-dihydro-1Hbenzo[d]-imidazole
bpy	2,2′-bipyridine
ppy	2-phenylpyridine
dcbpy	2,2′-bipyridine-5,5′-dicarboxylate
g-C_3N_4	Carbon nitride
ZIF	Zeolitic imidazolate framework
MCF	Mesoporous carbon flakes
EY	Eosin-Y
N-TC	N-doped TiO_2/C support
MO	Methyl orange
TiATA	Ti-MOF
Cu-PS	Photosensitizing linkers
UMOFN	2d Co-Ni-based MOF

References

1. Schlapbach L, Züttel A. Hydrogen-storage materials for mobile applications. Nature, 2001, 414(6861): 353–358
2. Nikolaidis P, Poullikkas A. A comparative overview of hydrogen production processes. Renewable & Sustainable Energy Reviews, 2017, 67: 597–611
3. Zhu J, Hu L, Zhao P, et al. Recent advances in electrocatalytic hydrogen evolution using nanoparticles. Chemical Reviews, 2020, 120(2): 851–918
4. Kandi D, Martha S, Parida K M. Quantum dots as enhancer in photocatalytic hydrogen evolution: a review. International Journal of Hydrogen Energy, 2017, 42(15): 9467–9481
5. Yu J, Yu X. Hydrothermal synthesis and photocatalytic activity of zinc oxide hollow spheres. Environmental Science & Technology, 2008, 42(13): 4902–4907
6. Dhanalakshmi K. Dye sensitized hydrogen evolution from water. International Journal of Hydrogen Energy, 2001, 26(7): 669–674
7. Al-Mamun M R, Kader S, Islam M S, et al. Photocatalytic activity improvement and application of UV-TiO_2 photocatalysis in textile wastewater treatment: a review. Journal of Environmental Chemical Engineering, 2019, 7(5): 103248
8. Ong C B, Ng L Y, Mohammad A W. A review of ZnO nanoparticles as solar photocatalysts: synthesis, mechanisms and applications. Renewable & Sustainable Energy Reviews, 2018, 81: 536–551
9. Huerta-Flores A M, Torres-Martínez L M, Moctezuma E, et al. Novel $SrZrO_3$-Sb_2O_3 heterostructure with enhanced photocatalytic activity: band engineering and charge transference mechanism. Journal of Photochemistry and Photobiology A Chemistry, 2018, 356: 166–176
10. Xing X, Wang D, Ye X, et al. The crystal structure and photocatalytic properties of a one-dimensional Zinc(II) coordination complex. Journal of Molecular Structure, 2019, 1183: 224–229
11. Sheng J, Dong H, Meng X, et al. Effect of different functional groups on photocatalytic hydrogen evolution in covalent-organic frameworks. ChemCatChem, 2019, 11(9): 2313–2319
12. Li H, Sun Y, Yuan Z, et al. Titanium phosphonate based metal–organic frameworks with hierarchical porosity for enhanced photocatalytic hydrogen evolution. Angewandte Chemie International Edition, 2018, 57(12): 3222–3227
13. Dinolfo P H, Hupp J T. Supramolecular coordination chemistry and functional microporous molecular materials. Chemistry of Materials, 2001, 13(10): 3113–3125
14. Hashemi B, Zohrabi P, Raza N, et al. Metal-organic frameworks as advanced sorbents for the extraction and determination of pollutants from environmental, biological, and food media. Trends in Analytical Chemistry, 2017, 97: 65–82
15. Meng J, Liu X, Niu C, et al. Advances in metal–organic framework coatings: versatile synthesis and broad applications. Chemical Society Reviews, 2020, 49(10): 3142–3186
16. Wade C R, Dincă M. Investigation of the synthesis, activation, and isosteric heats of CO_2 adsorption of the isostructural series of metal-organic frameworks $M_3(BTC)_2$ (M = Cr, Fe, Ni, Cu, Mo, Ru). Dalton Transactions: Cambridge, England: 2003, 2012, 41(26): 7931–7938
17. Zhang Y, Wang G, Ma W, et al. CdS p-n heterojunction co-boosting with Co_3O_4 and Ni-MOF-74 for photocatalytic hydrogen evolution. Dalton Transactions (Cambridge, England), 2018, 47(32): 11176–11189
18. Deng X, Albero J, Xu L, et al. Construction of a stable Ru–Re hybrid system based on multifunctional MOF-253 for efficient photocatalytic CO_2 reduction. Inorganic Chemistry, 2018, 57(14): 8276–8286
19. Zhao H, Xia Q, Xing H, et al. Construction of pillared-layer MOF

as efficient visible-light photocatalysts for aqueous Cr(VI) reduction and dye degradation. ACS Sustainable Chemistry & Engineering, 2017, 5(5): 4449–4456

20. Syzgantseva M A, Stepanov N F, Syzgantseva O A. Band alignment as the method for modifying electronic structure of metal-organic frameworks. ACS Applied Materials & Interfaces, 2020, 12(15): 17611–17619
21. Hasan Z, Jhung S H. Removal of hazardous organics from water using metal-organic frameworks (MOFs): plausible mechanisms for selective adsorptions. Journal of Hazardous Materials, 2015, 283: 329–339
22. Wu P, Jiang M, Li Y, et al. Highly efficient photocatalytic hydrogen production from pure water via a photoactive metal–organic framework and its PDMS@MOF. Journal of Materials Chemistry. A, Materials for Energy and Sustainability, 2017, 5(17): 7833–7838
23. Feng L, Wang K, Day G S, et al. Destruction of metal–organic frameworks: positive and negative aspects of stability and lability. Chemical Reviews, 2020, 120(23): 13087–13133
24. Jayaramulu K, Geyer F, Schneemann A, et al. Hydrophobic metal–organic frameworks. Advanced Materials, 2019, 31(32): 1900820
25. Alfonso-Herrera L A, Huerta-Flores A M, Torres Martínez L M, et al. M-008: a stable and reusable metalorganic framework with high crystallinity applied in the photocatalytic hydrogen evolution and the degradation of methyl orange. Journal of Photochemistry and Photobiology A, Chemistry, 2020, 389: 112240
26. An Y, Liu Y, Bian H, et al. Improving the photocatalytic hydrogen evolution of UiO-67 by incorporating Ce^{4+}-coordinated bipyridinedicarboxylate ligands. Science Bulletin, 2019, 64(20): 1502–1509
27. Li J, Huang H, Liu P, et al. Metal-organic framework encapsulated single-atom Pt catalysts for efficient photocatalytic hydrogen evolution. Journal of Catalysis, 2019, 375: 351–360
28. Zhang R, Liu Y, Wang J, et al. Post-synthetic platinum complex modification of a triazine based metal organic frameworks for enhanced photocatalytic H_2 evolution. Journal of Solid State Chemistry, 2019, 271: 260–265
29. Li S, Mei H, Yao S, et al. Well-distributed Pt-nanoparticles within confined coordination interspaces of self-sensitized porphyrin metal–organic frameworks: synergistic effect boosting highly efficient photocatalytic hydrogen evolution reaction. Chemical Science (Cambridge), 2019, 10(45): 10577–10585
30. Alfonso Herrera L Á, Camarillo Reyes P K, Huerta Flores A M, et al. BDC-Zn MOF sensitization by MO/MB adsorption for photocatalytic hydrogen evolution under solar light. Materials Science in Semiconductor Processing, 2020, 109: 104950
31. Yang H, Wang J, Ma J, et al. A novel BODIPY-based MOF photocatalyst for efficient visible-light-driven hydrogen evolution. Journal of Materials Chemistry. A, Materials for Energy and Sustainability, 2019, 7(17): 10439–10445
32. Pi Y, Feng X, Song Y, et al. Metal-organic frameworks integrate Cu photosensitizers and secondary building unit-supported Fe catalysts for photocatalytic hydrogen evolution. Journal of the American Chemical Society, 2020, 142(23): 10302–10307
33. Song Y, Li Z, Zhu Y, et al. Titanium hydroxide secondary building units in metal-organic frameworks catalyze hydrogen evolution under visible light. Journal of the American Chemical Society, 2019, 141(31): 12219–12223
34. Wang J, Cherevan A S, Hannecart C, et al. Ti-based MOFs: new insights on the impact of ligand composition and hole scavengers on stability, charge separation and photocatalytic hydrogen evolution. Applied Catalysis B: Environmental, 2021, 283: 119626
35. Liang Y, Shang R, Lu J, et al. 2D MOFs enriched g-C_3N_4 nanosheets for highly efficient charge separation and photocatalytic hydrogen evolution from water. International Journal of Hydrogen Energy, 2019, 44(5): 2797–2810
36. Gao Z, Wang L, Wang L, et al. Construction of heterostructured g-C_3N_4@TiATA/Pt composites for efficacious photocatalytic hydrogen evolution. International Journal of Hydrogen Energy, 2019, 44(45): 24407–24417
37. Li M, Li J, Jin Z. 0D/2D spatial structure of $Cd_xZn_{1-x}S$/Ni-MOF-74 for efficient photocatalytic hydrogen evolution. Dalton Transactions (Cambridge, England), 2020, 49(16): 5143–5156
38. Sun L, Yuan Y, Wang F, et al. Selective wet-chemical etching to create TiO_2@MOF frame heterostructure for efficient photocatalytic hydrogen evolution. Nano Energy, 2020, 74: 104909
39. Ren R, Zhao H, Sui X, et al. Exfoliated molybdenum disulfide encapsulated in a metal organic framework for enhanced photocatalytic hydrogen evolution. Catalysts, 2019, 9(1): 89
40. Zhang H, Yang Y, Li C, et al. A new strategy for constructing covalently connected MOF@COF core–shell heterostructures for enhanced photocatalytic hydrogen evolution. Journal of Materials Chemistry. A, Materials for Energy and Sustainability, 2021, 9(31): 16743–16750
41. Aleksandrzak M, Baranowska D, Kedzierski T, et al. Superior synergy of g-C_3N_4/Cd compounds and Al-MOF-derived nanoporous carbon for photocatalytic hydrogen evolution. Applied Catalysis B: Environmental, 2019, 257: 117906
42. Xu J, Qi Y, Wang L. *In situ* derived Ni_2P/Ni encapsulated in carbon/g-C_3N_4 hybrids from metal-organic frameworks/g-C_3N_4 for efficient photocatalytic hydrogen evolution. Applied Catalysis B: Environmental, 2019, 246: 72–81
43. Li N, Huang H, Bibi R, et al. Noble-metal-free MOF derived hollow CdS/TiO_2 decorated with NiS cocatalyst for efficient photocatalytic hydrogen evolution. Applied Surface Science, 2019, 476: 378–386
44. Lin L, Huang S, Zhu Y, et al. Construction of CdS/MoS_2 heterojunction from core-shell MoS_2@Cd-MOF for efficient photocatalytic hydrogen evolution. Dalton Transactions, 2019, 48(8): 2715–2721
45. Zhang L, Wang G, Hao X, et al. MOFs-derived Cu_3P@CoP p-n heterojunction for enhanced photocatalytic hydrogen evolution. Chemical Engineering Journal, 2020, 395: 125113
46. Yan B, Liu D, Feng X, et al. Ru species supported on MOF-derived N-doped TiO_2/C hybrids as efficient electrocatalytic/photocatalytic hydrogen evolution reaction catalysts. Advanced Functional Materials, 2020, 30(31): 2003007
47. Xiao Y, Wang X, Yu H, et al. MOF-5 derived C-doped ZnO decorated with Cu cocatalyst for enhancing visible-light driven

photocatalytic hydrogen evolution. Journal of Physics and Chemistry of Solids, 2021, 149: 109793

48. Huerta-Flores A M, Torres-Martínez L M, Sánchez-Martínez D, et al. $SrZrO_3$ powders: alternative synthesis, characterization and application as photocatalysts for hydrogen evolution from water splitting. Fuel, 2015, 158: 66–71
49. Feng X, Pi Y, Song Y, et al. Metal-organic frameworks significantly enhance photocatalytic hydrogen evolution and CO_2 reduction with earth-abundant copper photosensitizers. Journal of the American Chemical Society, 2020, 142(2): 690–695
50. Talin A A, Centrone A, Ford A C, et al. Tunable electrical conductivity in metal-organic framework thin-film devices. Science, 2014, 343(6166): 66–69
51. Seal N, Goswami R, Singh M, et al. An ultralight charged MOF as fluoro-switchable monitor for assorted organo-toxins: size-exclusive dye scrubbing and anticounterfeiting applications via Tb^{3+} sensitization. Inorganic Chemistry Frontiers, 2021, 8(2): 296–310
52. Loera-Serna S, Ortiz E, Beltrán H I. First trial and physicochemical studies on the loading of basic fuchsin, crystal violet and Black Eriochrome T on HKUST-1. New Journal of Chemistry, 2017, 41(8): 3097–3105
53. Li C, Qiu W, Long W, et al. Synthesis of porphyrin@MOFs type catalysts through “one-pot” self-assembly. Journal of Molecular Catalysis A Chemical, 2014, 393: 166–170
54. Yan A X, Yao S, Li Y G, et al. Incorporating polyoxometalates into a porous MOF greatly improves its selective adsorption of cationic dyes. Chemistry (Weinheim an der Bergstrasse, Germany), 2014, 20(23): 6927–6933
55. Esken D, Zhang X, Lebedev O I, et al. Pd@MOF-5: limitations of gas-phase infiltration and solution impregnation of $[Zn_4O(bdc)_3]$ (MOF-5) with metal–organic palladium precursors for loading with Pd nanoparticles. Journal of Materials Chemistry, 2009, 19(9): 1314–1319
56. Kumar S, Kumar A, Kumar A, et al. Nanoscale zinc oxide based heterojunctions as visible light active photocatalysts for hydrogen energy and environmental remediation. Catalysis Reviews. Science and Engineering, 2020, 62(3): 346–405
57. Vattikuti S V P. Chapter 4 - heterostructured nanomaterials: latest trends in formation of inorganic heterostructures. In: Bhagyaraj S M, Oluwafemi O S, eds. Synthesis of Inorganic Nanomaterials. Woodhead Publishing, 2018: 89–120
58. Li Y, Li X, Zhang H, et al. Design and application of active sites in g-C_3N_4-based photocatalysts. Journal of Materials Science and Technology, 2020, 56: 69–88
59. Liu J, Fu W, Liao Y, et al. Recent advances in crystalline carbon nitride for photocatalysis. Journal of Materials Science and Technology, 2021, 91: 224–240
60. Luo B, Zhao Y, Jing D. State-of-the-art progress in overall water splitting of carbon nitride based photocatalysts. Frontiers in Energy, 2021, 15(3): 600–620
61. Butler K T, Hendon C H, Walsh A. Designing porous electronic thin-film devices: band offsets and heteroepitaxy. Faraday Discussions, 2017, 201: 207–219